Frontiers of Information Technology & Electronic Engineering
www.jzus.zju.edu.cn; engineering.cae.cn; www.springerlink.com
ISSN 2095-9184 (print); ISSN 2095-9230 (online)
E-mail: jzus@zju.edu.cn

A non-stationary channel model for 5G massive MIMO systems*

Jian-qiao CHEN‡, Zhi ZHANG, Tian TANG, Yu-zhen HUANG

(*Department of Information and Communication Engineering, Beijing University of Posts and Telecommunications, Beijing 100876, China*)

E-mail: jqchen1988@163.com; zhangzhi@bupt.edu.cn; tangtian@bupt.edu.cn; yzh_huang@sina.com

Received Jan. 13, 2017; Revision accepted Apr. 23, 2017; Crosschecked Dec. 20, 2017

Abstract: We propose a novel channel model for massive multiple-input multiple-out (MIMO) communication systems that incorporate the spherical wave-front assumption and non-stationary properties of clusters on both the array and time axes. Because of the large dimension of the antenna array in massive MIMO systems, the spherical wave-front is assumed to characterize near-field effects resulting in angle of arrival (AoA) shifts and Doppler frequency variations on the antenna array. Additionally, a novel visibility region method is proposed to capture the non-stationary properties of clusters at the receiver side. Combined with the birth-death process, a novel cluster evolution algorithm is proposed. The impacts of cluster evolution and the spherical wave-front assumption on the statistical properties of the channel model are investigated. Meanwhile, corresponding to the theoretical model, a simulation model with a finite number of rays that capture channel characteristics as accurately as possible is proposed. Finally, numerical analysis shows that our proposed non-stationary channel model is effective in capturing the characteristics of a massive MIMO channel.

Key words: Massive MIMO; Spherical wave-front assumption; Non-stationary property; Birth-death process; Visibility region method

https://doi.org/10.1631/FITEE.1700028 **CLC number:** TN929.5

1 Introduction

Recently, massive multiple-input multiple-output (MIMO) has been proposed as one of the essential candidate technologies for the fifth generation (5G) wireless communication networks (Larsson *et al.*, 2014; Wang *et al.*, 2014; Zheng *et al.*, 2014). Compared to the conventional MIMO system, it is equipped with tens or even hundreds of antennas to serve users in the same time-frequency slot. Many excellent features make the massive MIMO attractive, such as very high spectral efficiency and capacity, significantly increased energy efficiency, and a low-complexity processing interference (Rusek *et al.*, 2013; Lu *et al.*, 2014). As a result, massive MIMO technology has good prospects in future wireless communication systems.

For MIMO system design and performance evaluation, an accurate small-scale fading MIMO channel model is indispensable. As to conventional MIMO systems, channel models known as geometry-based stochastic models (GBSMs) are widely studied. The GBSM is beneficial from its extensive applicability, because it models the locations of clusters according to a certain probability distribution rather than a specific channel environment. Many analytical and standard GBSMs have been proposed (Kyösti *et al.*, 2007; ITU-R, 2008; Paetzold, 2011; ETSI, 2014). However, according to the channel

‡ Corresponding author

* Project supported by the National Natural Science Foundation of China (No. 61421061) and the Huawei Innovation Research Program

ORCID: Jian-qiao CHEN, http://orcid.org/0000-0003-3491-9237

measurements in Gao *et al.* (2012) and Payami and Tufvesson (2012), there are two characteristics that make the conventional MIMO channel models not effective for application to model massive MIMO channels directly. First, the far-field propagation assumption (always defined to be greater than the Rayleigh distance (Yaghjian, 1986)) is no longer valid with a large number of antennas. Therefore, the wave-front should be assumed as spherical instead of plane. The effect of the spherical wave-front assumption was analyzed in Bohagen *et al.* (2006).

Second, non-stationary properties of clusters can be observed on large antenna arrays. In other words, different antenna elements may observe different sets of clusters. Thus, the wide-sense stationary (WSS) assumption of clusters for conventional MIMO is not satisfied for massive MIMO channels. The methods of describing non-stationary properties of clusters can be divided mainly into two categories: the birth-death process and visibility region method. The birth-death process is introduced to describe cluster evolution on the time axis (Babich and Lombardi, 2000; Zwick *et al.*, 2000, 2002; Chong *et al.*, 2005) at first, and then it is extended to the antenna array (Wu SB *et al.*, 2014, 2015; Wu HL *et al.*, 2015). In these channel models, the cluster evolves separately on the transmit and receive antennas based on the birth-death process, and then existing clusters are randomly paired to determine to which transmit and receive antennas each cluster is observable. A brief description of the algorithm flow is shown in Section 2. Although cluster evolution based on the birth-death process has proved effective, it has disadvantages, such as its complexity and time-consuming theoretical analysis, and its lack of intuitive geometric characteristics between clusters and the antenna array. The visibility region method has been widely investigated (Liu *et al.*, 2012; Gao *et al.*, 2013; Li *et al.*, 2015; Xie *et al.*, 2015), and different definitions of the visibility region determine different methods of describing cluster evolution. The visibility region is typically assigned to a geometric region in which the antenna is visible to the corresponding cluster, and the cluster is active (contributing to the impulse response) upon entering the visibility region. From this perspective, the visibility region method is more naturally integrated into the channel model based on stochastic geometry.

In this paper, a novel scheme is proposed to capture the spherical wave-front effect and non-stationary properties of clusters on both the array and time axes for the massive MIMO channel model. This paper is summarized as follows. First, assuming a spherical wave-front, expressions for calculating AoA shifts, Doppler frequencies, and channel coefficients are derived in detail, including the line-of-sight (LOS) and non-line-of-sight (NLOS) components. Second, a novel visibility region method is proposed to describe cluster evolution on the receive antenna; then, combined with the birth-death process, a novel cluster evolution algorithm is given. Third, the impacts of the spherical wave-front assumption and cluster evolution on the statistical properties of our proposed model are investigated. A corresponding simulation model for the theoretical model with a finite number of rays is proposed.

2 Preliminaries of the birth-death process

The birth-death process can effectively reproduce the non-stationary properties of clusters in massive MIMO channels on both the array and time axes. Assume the initial number of clusters N and the initial cluster set of the first transmit (receive) antenna $C_1 = \{c_x \mid x = 1, 2, \ldots, N\}$ at the initial time instant t are given, where c_x represents Cluster_x, and the subscript x represents the xth cluster in the cluster set. The clusters in cluster set C_1 evolve according to the birth-death process to recursively generate cluster sets of the rest of the antennas at the transmitter (receiver) side at the initial time t, i.e., $C_{n-1}(t) \xrightarrow{E} C_n(t)$, $(n = 2, 3, \ldots)$, where the operator $\xrightarrow{E}$ denotes cluster evolution on either the array or time axis. Cluster evolution on both the array and time axes is determined by the cluster generation rate and the recombination rate. As the cluster evolution occurs, the disappearing cluster members are eliminated from all cluster sets, and the newly generated cluster members are added to corresponding cluster sets. Because each cluster evolves gradually on both the array and time axes, it will not appear again after its disappearance. Therefore, antenna correlations are naturally embedded in the generation process.

3 Theoretical non-stationary massive MIMO channel model

3.1 Channel impulse response

Our proposed channel model for massive MIMO is illustrated in Fig. 1. When calculating the channel impulse response, two important characteristics should be considered in massive MIMO channels. First, the far-field assumption for conventional MIMO channel models is not fulfilled as the dimension of the antenna array becomes large. As a result, the wave-front should be assumed to be spherical. An example of the nth cluster of the receive antenna array is shown in Fig. 1. The spherical wave-front of each wireless link results in AoA shifts and the Doppler frequencies on the antenna array are no longer the same for each antenna element. Therefore, they should be determined by geometrical relationships. Second, the non-stationary properties of clusters on the antenna array mean that a cluster may be observed only by a partial set of antennas on the antenna array in massive MIMO channel models. Let $\mathrm{Ant}_l^{\mathrm{T}}$ represent the lth antenna of the transmit array and $\mathrm{Ant}_k^{\mathrm{R}}$ represent the kth antenna of the receive array. Examples are given in Fig. 1. On one hand, $\mathrm{Cluster}_{n+1}$ is observed by $\mathrm{Ant}_l^{\mathrm{T}}$ but is not observed by $\mathrm{Ant}_k^{\mathrm{R}}$. Conversely, $\mathrm{Cluster}_{n+2}$ is observed by $\mathrm{Ant}_k^{\mathrm{R}}$ but is not observed by $\mathrm{Ant}_l^{\mathrm{T}}$. On the other hand, $\mathrm{Cluster}_n$ is observed by both $\mathrm{Ant}_l^{\mathrm{T}}$ and $\mathrm{Ant}_k^{\mathrm{R}}$. These situations imply that different antenna elements may observe different sets of clusters.

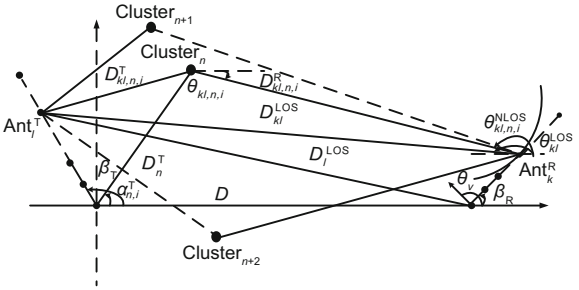

Fig. 1 A theoretical channel model for massive MIMO systems

Assume that the transmitter and receiver are equipped with uniform linear arrays (ULAs) with M_{T} and M_{R} omnidirectional antenna elements, respectively. The coordinates of $\mathrm{Ant}_1^{\mathrm{T}}$ and $\mathrm{Ant}_1^{\mathrm{R}}$ are $(0,0)$ and $(D,0)$, respectively, where D is the horizontal distance between the transmitter and receiver. The maximum Doppler frequency and carrier wavelength are denoted as $f_{\max}$ and λ, respectively. The counterclockwise direction is considered as the positive direction. Key parameter definitions are given in Table 1. Assume that the mean power of the nth cluster is P_n, the LOS Rician factor is K, and each cluster consists of M rays. The channel coefficient $h_{kl,n}(t)$ of the $\mathrm{Cluster}_n$ between $\mathrm{Ant}_l^{\mathrm{T}}$ and $\mathrm{Ant}_k^{\mathrm{R}}$ is presented as

$$h_{kl,n}(t)=\underbrace{\delta(n-1)\sqrt{\frac{K}{K+1}}\exp\left(\mathrm{j}(2\pi f_{kl}^{\mathrm{LOS}}t+\varphi_{kl}^{\mathrm{LOS}})\right)}_{\mathrm{LOS}}+\underbrace{\sqrt{\frac{P_n}{K+1}}\lim_{M\to\infty}\frac{1}{\sqrt{M}}\sum_{i=1}^{M}\exp\left(\mathrm{j}(2\pi f_{kl,n,i}^{\mathrm{NLOS}}+\varphi_{kl,n,i}^{\mathrm{NLOS}})\right)}_{\mathrm{NLOS}}. \tag{1}$$

The calculation of channel coefficients can be divided into the LOS component and NLOS component. For the LOS component, the received phase of $\mathrm{Ant}_k^{\mathrm{R}}$ from $\mathrm{Ant}_l^{\mathrm{T}}$ can be expressed as

$$\varphi_{kl}^{\mathrm{LOS}}=\varphi_0+\frac{2\pi}{\lambda}(D_{kl}^{\mathrm{LOS}}-D_l^{\mathrm{LOS}}), \tag{2}$$

where

$$\begin{aligned}D_{kl}^{\mathrm{LOS}}=&\\&\{[(l-1)\delta_{\mathrm{T}}\cos(\beta_{\mathrm{T}})-(k-1)\delta_{\mathrm{R}}\cos(\beta_{\mathrm{R}})-D]^2\\&+[(l-1)\delta_{\mathrm{T}}\sin(\beta_{\mathrm{T}})-(k-1)\delta_{\mathrm{R}}\sin(\beta_{\mathrm{R}})]^2\}^{1/2},\end{aligned} \tag{3}$$

$$\begin{aligned}D_l^{\mathrm{LOS}}=\{&[(l-1)\delta_{\mathrm{T}}\cos(\beta_{\mathrm{T}})-D]^2\\&+[(l-1)\delta_{\mathrm{T}}\sin(\beta_{\mathrm{T}})]^2\}^{1/2}.\end{aligned} \tag{4}$$

The AoA of the LOS component from $\mathrm{Ant}_l^{\mathrm{T}}$ to $\mathrm{Ant}_k^{\mathrm{R}}$ can be computed as

$$\theta_{kl}^{\mathrm{LOS}}=\arcsin\left(\frac{(k-1)\delta_{\mathrm{R}}\sin(\beta_{\mathrm{R}})-(l-1)\delta_{\mathrm{T}}\sin(\beta_{\mathrm{T}})}{D_{kl}^{\mathrm{LOS}}}\right). \tag{5}$$

The Doppler frequency of the LOS component between $\mathrm{Ant}_l^{\mathrm{T}}$ and $\mathrm{Ant}_k^{\mathrm{R}}$ can be computed as

$$f_{kl}^{\mathrm{LOS}}=f_{\max}\cos(\theta_v-\theta_{kl}^{\mathrm{LOS}}). \tag{6}$$

For the NLOS component, the received phase of $\mathrm{Ant}_k^{\mathrm{R}}$ from $\mathrm{Ant}_l^{\mathrm{T}}$ via the ith ray within the nth cluster can be expressed as

$$\varphi_{kl,n,i}^{\mathrm{NLOS}}=\varphi_0+\frac{2\pi}{\lambda}(D_{kl,n,i}^{\mathrm{T}}+D_{kl,n,i}^{\mathrm{R}}), \tag{7}$$

where

$$\begin{aligned}D_{kl,n,i}^{\mathrm{T}}=&\{[D_n^{\mathrm{T}}\cos(\alpha_{n,i}^{\mathrm{T}})-(l-1)\delta_{\mathrm{T}}\cos(\beta_{\mathrm{T}})]^2\\&+[D_n^{\mathrm{T}}\sin(\alpha_{n,i}^{\mathrm{T}})-(l-1)\delta_{\mathrm{T}}\sin(\beta_{\mathrm{T}})]^2\}^{1/2},\end{aligned} \tag{8}$$

Table 1 Definition of key geometry parameters

Symbol	Description
$\delta_{\mathrm{T}}(\delta_{\mathrm{R}})$	Antenna spacing of the transmit (receive) antenna array
$\beta_{\mathrm{T}}(\beta_{\mathrm{R}})$	Tilt angles of the transmit (receive) antenna array
$l(k), M_{\mathrm{T}}(M_{\mathrm{R}})$	The index of the transmit (receive) antenna and total number of transmit (receive) antennas
D_n^{T}	Distance between the nth cluster and the first transmit antenna
D_l^{LOS}	LOS distance between the lth transmit antenna and the first receive antenna
D_{kl}^{LOS}	LOS distance between the lth transmit antenna and the kth receive antenna
$D_{kl,n,i}^{\mathrm{T}}$	Distance between the nth cluster and the lth transmit antenna via the ith ray
$D_{kl,n,i}^{\mathrm{R}}$	Distance between the nth cluster and the kth receive antenna via the ith ray
$\theta_{kl}^{\mathrm{LOS}}$	AoA of the LOS component from the lth transmit to the kth receive antenna
$\theta_{kl,n,i}^{\mathrm{NLOS}}$	AoA from the lth transmit and the kth receive antenna via the ith ray within the nth cluster
$\alpha_{n,i}^{\mathrm{T}}$	Angle of departure (AoD) from the first transmit antenna to the nth cluster via the ith ray
θ_v	Direction of movement of the receive antenna

$$D_{kl,n,i}^{\mathrm{R}} = \{[D_n^{\mathrm{T}}\cos(\alpha_{n,i}^{\mathrm{T}}) - (k-1)\delta_{\mathrm{R}}\cos(\beta_{\mathrm{R}}) - D]^2 + [D_n^{\mathrm{T}}\sin(\alpha_{n,i}^{\mathrm{T}}) - (k-1)\delta_{\mathrm{R}}\sin(\beta_{\mathrm{R}})]^2\}^{1/2}. \quad (9)$$

The AoA of the ith ray within the nth cluster from $\mathrm{Ant}_l^{\mathrm{T}}$ to $\mathrm{Ant}_k^{\mathrm{R}}$ can be computed as

$$\theta_{kl,n,i}^{\mathrm{NLOS}} = \arcsin\left(\frac{(k-1)\delta_{\mathrm{R}}\sin(\beta_{\mathrm{R}}) - D_n^{\mathrm{T}}\sin(\alpha_{n,i}^{\mathrm{T}})}{D_{kl,n,i}^{\mathrm{R}}}\right). \quad (10)$$

The Doppler frequency of the ith ray within the nth cluster from $\mathrm{Ant}_l^{\mathrm{T}}$ to $\mathrm{Ant}_k^{\mathrm{R}}$ can be computed as

$$f_{kl,n,i}^{\mathrm{NLOS}} = f_{\max}\cos(\theta_v - \theta_{kl,n,i}^{\mathrm{NLOS}}). \quad (11)$$

3.2 Clusters evolution on the array axis

So far, the impulse responses of the proposed model have been derived in detail from Eqs. (1)–(11) based on geometric relationships. However, Eq. (1) holds if and only if $\mathrm{Cluster}_n \in \{C_l^{\mathrm{T}} \cap C_k^{\mathrm{R}}\}$, where C_l^{T} and C_k^{R} represent the cluster set in which clusters are observed by $\mathrm{Ant}_l^{\mathrm{T}}$ to $\mathrm{Ant}_k^{\mathrm{R}}$, respectively. In this section, we propose a novel visibility region method to describe the cluster evolution at the receiver side. Then, combined with the birth-death process at the transmitter side, a novel cluster evolution algorithm is proposed (Algorithm 1). The time index is temporarily dropped because cluster evolution on the time axis is not considered in this subsection. The process of cluster evolution on the array axis includes two parts.

1. Clusters evolve on the transmit antenna array according to the birth-death process, which has been widely investigated in articles (Wu SB *et al.*, 2014, 2015; Wu HL *et al.*, 2015). First, assume the initial number of clusters is N and the initial cluster set of the first transmit antenna $C_1^{\mathrm{T}} = \{c_x^{\mathrm{T}} \mid x = 1, 2, \ldots, N\}$ is given, where c_x^{T} is a representation of $\mathrm{Cluster}_x$ corresponding to the first transmit

Algorithm 1 Evolution process of rays within clusters

Input: set the initial parameters of C_1^{T}, and evolve on the transmit antenna array to recursively generate the cluster sets of the rest of the antennas according to the birth-death process.

for number of transmit antennas $l \in [1, M_{\mathrm{T}}]$ **do**
  for number of clusters in the cluster set C_l^{T} **do**
    Set the total number of rays within the cluster, and compute the offset angles of rays according to the uniform power sub-path method;
    for number of rays within the nth cluster $i \in [1, M]$ **do**
      for number of receive antennas $k \in [1, M_{\mathrm{R}}]$ **do**
        Compute distance between the lth transmit antenna and the nth cluster via the ith ray;
        Compute distance between the kth receive antenna and the nth cluster via the ith ray;
        Compute the power distribution against emitted direction via the ith ray under the given PAS;
        Compute the visibility gain of the ith ray corresponding to the kth receive antenna;
        Set a threshold and if visibility gain exceeds the threshold, the ith ray will be added to the ray sets visible to the kth receive antenna;
      end for
    end for
  end for
end for

Output: C_l^{T} $(l = 1, 2, \ldots, M_{\mathrm{T}})$.

antenna. The position of c_x^{T} can be determined by the AoD of Cluster$_x$ and the distance between the Cluster$_x$ and the origin of coordinates. These two initial parameters can be generated according to statistical distribution. Herein, let us assume that the distance satisfies the uniform distribution $U(0,25)$, and AoD satisfies the wrapped Gaussian distribution $N(0.78,0.11^2)$, which is based on the standard WINNER II channel model (Kyösti *et al.*, 2007). Then, the clusters in cluster set C_1^{T} evolve on the array axis to recursively generate the cluster sets of the rest of the antennas according to the birth-death process, namely $C_{l-1}^{\mathrm{T}}(t) \xrightarrow{E} C_l^{\mathrm{T}}(t)$ $(l=2,3,\ldots,M_{\mathrm{T}})$.

2. Herein, a novel visibility region method is proposed to describe cluster evolution on the receive antenna array after cluster sets C_l^{T} have been obtained. In general, a cluster is composed of some rays, which are distinguished from each other by different angles. Thus, it is more reasonable to describe a visibility region in terms of the ray rather than the cluster. Specifically, clusters can be divided into three categories according to the visibility of rays: a wholly visible (WV) cluster means that all the rays within the cluster are visible to the antenna array; a partially visible (PV) cluster means that only part of rays within the cluster are visible to the antenna array; a wholly invisible (WIV) cluster means that all the rays are invisible to the antenna array. An illustration of the WV cluster and PV cluster is shown in Fig. 2. As a result, non-stationary properties can be modeled by incorporating the WV and PV clusters and their corresponding parameters.

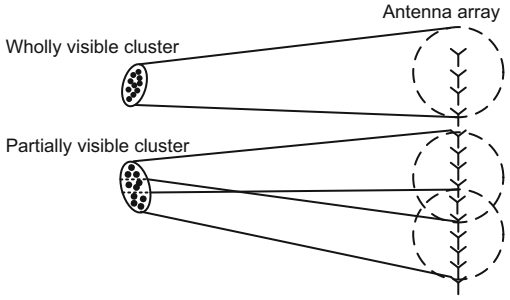

Fig. 2 Illustration of the visible region from the ray perspective

In our proposed scheme, the cluster visibility region is described by gains in the visibility of rays within the cluster, which depend on two aspects: the emitting direction from the transmit antenna to the receive antenna via the ray, and the distance between the transmit antenna and the receive antenna via the ray. Due to re-radiation of a scatterer, many rays with different offset angles within a cluster are generated. Therefore, the number of rays and the offset angles of rays should be determined first. Similar to the 3GPP spatial channel model (ETSI, 2014), the uniform power subpath method is used to calculate offset angles of rays, which are based on the condition of the area of each section, when each ray is equally divided under the power azimuth spectrum (PAS). To ensure that the areas of sections divided by two subsequent offset angles are equal, the area of section under the given PAS can be expressed as

$$\int_{\theta_1}^{\theta_2} \mathrm{PAS}(\theta,\sigma)\mathrm{d}\theta = \frac{1}{a(M+1)}, \tag{12}$$

where θ_1 and θ_2 denote the offset angles of adjacent rays, σ is the root mean square (RMS) angular spread (AS), M is the total number of rays, and a is the normalization factor. If M is odd, $a=1$; otherwise, $a=2$.

After obtaining the offset angles of rays, the emitting direction from the transmit antenna via the ray can be determined. Due to the re-radiation of the same scatterer, it can be considered that the emitting direction of rays through the scatterer will satisfy the same power distribution function. So, some kind of PAS will be adopted to describe the power distribution against the emitting direction of rays, such as a Laplacian distribution, Gaussian distribution, or uniform distribution (Schumacher *et al.*, 2002). Finally, together with logarithmic functions, which can be used to describe the path-loss between the transmit antenna and receive antenna via the ray, the cluster visibility gain can be calculated. Let us take the Laplacian PAS and free space path-loss function as an example. The visibility gain of the ith ray within the nth cluster can be expressed as

$$\begin{aligned}\mathrm{Gain} = {} & \mathrm{PL}(D_{kl,n,i}^{\mathrm{T}}) + \mathrm{PL}(D_{kl,n,i}^{\mathrm{R}}) \\ & + [P_{\mathrm{init}} - \mathrm{PL}(D_{kl,n,i}^{\mathrm{T}})] \cdot \mathrm{PAS}(\theta_{kl,n,i},\sigma),\end{aligned} \tag{13}$$

$$\mathrm{PAS}(\theta,\sigma) = \frac{Q}{\sqrt{2}\sigma}\exp\left(-\frac{\sqrt{2}|\theta-\theta_0|}{\sigma}\right), \quad \text{with } \theta_0-\Delta\theta \le \theta \le \theta_0+\Delta\theta, \tag{14}$$

$$\mathrm{PL}(d) = 20\lg\left(\frac{4\pi d}{\lambda}\right), \tag{15}$$

$$\theta_{kl,n,i} = \pi - |\theta_{kl,n,i}^{\mathrm{NLOS}}|, \tag{16}$$

$$\alpha_{n,i}^{\mathrm{T}}=\alpha_n^{\mathrm{T}}+\Delta\theta_i,\ i=1,2,\ldots,M, \tag{17}$$

$$\Delta\theta_{i+1}=-\frac{1.29\sigma}{\sqrt{2}}\ln\left(\exp\left(-\frac{\sqrt{2}\Delta\theta_i}{\sigma}\right)-\frac{2}{a(M+1)}\right),\quad i=0,1,2,\ldots,\lfloor M/2\rfloor, \tag{18}$$

where calculations of $D_{kl,n,i}^{\mathrm{T}}$, $D_{kl,n,i}^{\mathrm{R}}$, and $\theta_{kl,n,i}^{\mathrm{NLOS}}$ are related to $\alpha_{n,i}^{\mathrm{T}}$, expressed in Eqs. (8)–(10), P_{init} is the initial power of the transmit antenna, Q is the normalization constant, θ_0 is the average angle, $\Delta\theta$ is the maximum value range, $\Delta\theta_i$ is the offset angle of the ith ray, and $\lfloor\cdot\rfloor$ indicates rounding down.

For each ray within the clusters in C_l^{T}, its visibility gain to the entire receive antenna array will be calculated according to Eq. (13). After a threshold is set, which can be determined through measurements in specific scenarios, the visibility of rays within the cluster can be judged. If the ray visibility gain to the receive antenna exceeds the threshold, it becomes visible and is added to the ray sets that are visible to the corresponding receive antenna. The complete algorithm for obtaining ray sets of the entire receive antenna array is shown in Algorithm 1.

3.3 Cluster evolution on both the array and time axes

By combining the birth-death process on the time axis in Zwick *et al.* (2002), cluster evolution on both the array and time axes can be established. In our scheme, the time-variant property of the channel is caused by the movement of both the receiver and clusters. Therefore, parameters D_n^{T}, $\alpha_{n,i}^{\mathrm{T}}$, $D_{kl,n,i}^{\mathrm{T}}$, $D_{kl,n,i}^{\mathrm{R}}$, and $\theta_{kl,n,i}^{\mathrm{NLOS}}$ become time-variant as $D_n^{\mathrm{T}}(t)$, $\alpha_{n,i}^{\mathrm{T}}(t)$, $D_{kl,n,i}^{\mathrm{T}}(t)$, $D_{kl,n,i}^{\mathrm{R}}(t)$, and $\theta_{kl,n,i}^{\mathrm{NLOS}}(t)$, respectively. In this case, two aspects should be considered. First, geometrical relationships among the transmitter, the receiver, and clusters need to be updated as time changes. Second, cluster sets of each antenna evolve with time either. $\mathrm{Cluster}_n$ and the receive antenna array move to new positions from t to $t+\Delta t$, as shown in Fig. 3. Assume $\mathrm{Cluster}_n$ moves in an arbitrary direction $\theta_{c,n}$ with a speed of v_c, then at $t+\Delta t$, the received phase of $\mathrm{Ant}_k^{\mathrm{R}}$ from $\mathrm{Ant}_l^{\mathrm{T}}$ via the ith ray within the nth cluster can be expressed as

$$\varphi_{kl,n,i}^{\mathrm{NLOS}}(t+\Delta t)=\varphi_0+\frac{2\pi}{\lambda}[D_{kl,n,i}^{\mathrm{T}}(t+\Delta t)+D_{kl,n,i}^{\mathrm{R}}(t+\Delta t)], \tag{19}$$

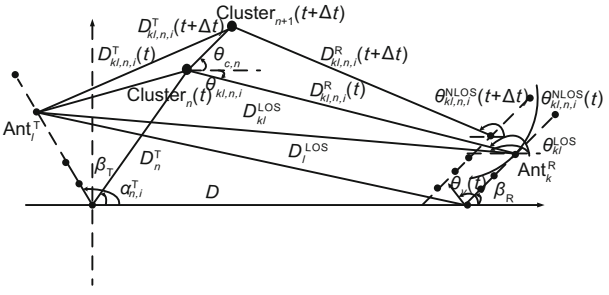

Fig. 3 Geometrical relationship evolution from t to $t+\Delta t$ of the proposed model

where

$$\begin{aligned}D_{kl,n,i}^{\mathrm{T}}(t+\Delta t)&=\{[D_n^{\mathrm{T}}(t)\cos(\alpha_{n,i}^{\mathrm{T}}(t))+v_c\Delta t\cos(\theta_{c,n})\\&\quad-(l-1)\delta_{\mathrm{T}}\cos(\beta_{\mathrm{T}})]^2+[D_n^{\mathrm{T}}(t)\sin(\alpha_{n,i}^{\mathrm{T}}(t))\\&\quad+v_c\Delta t\sin(\theta_{c,n})-(l-1)\delta_{\mathrm{T}}\sin(\beta_{\mathrm{T}})]^2\}^{1/2},\end{aligned} \tag{20}$$

$$\begin{aligned}D_{kl,n,i}^{\mathrm{R}}(t+\Delta t)&=\{[(k-1)\delta_{\mathrm{R}}\cos(\beta_{\mathrm{R}})+v\Delta t\cos(\theta_v)+D\\&\quad-D_n^{\mathrm{T}}(t)\cos(\alpha_{n,i}^{\mathrm{T}}(t))-v_c\Delta t\cos(\theta_{c,n})]^2\\&\quad+[(k-1)\delta_{\mathrm{R}}\sin(\beta_{\mathrm{R}})+v\Delta t\sin(\theta_v)\\&\quad-D_n^{\mathrm{T}}(t)\sin(\alpha_{n,i}^{\mathrm{T}}(t))-v_c\Delta t\sin(\theta_{c,n})]^2\}^{1/2}.\end{aligned} \tag{21}$$

The Doppler frequency of the ith ray within the nth cluster from $\mathrm{Ant}_l^{\mathrm{T}}$ to $\mathrm{Ant}_k^{\mathrm{R}}$ at $t+\Delta t$ can be expressed as

$$f_{kl,n,i}^{\mathrm{NLOS}}(t+\Delta t)=f_{\max}\cos(\theta_v-\theta_{kl,n,i}^{\mathrm{NLOS}}(t+\Delta t)), \tag{22}$$

where

$$\begin{aligned}\theta_{kl,n,i}^{\mathrm{NLOS}}(t+\Delta t)&=\arcsin\left[\frac{(k-1)\delta_{\mathrm{R}}\sin(\beta_{\mathrm{R}})+v\Delta t\sin(\theta_v)}{D_{kl,n,i}^{\mathrm{R}}(t+\Delta t)}\right.\\&\quad\left.-\frac{D_n^{\mathrm{T}}(t)\sin(\alpha_{n,i}^{\mathrm{T}}(t))+v_c\Delta t\sin(\theta_{c,n})}{D_{kl,n,i}^{\mathrm{R}}(t+\Delta t)}\right].\end{aligned} \tag{23}$$

In addition to geometrical relationships, cluster sets of each antenna evolve with time as well. As time changes, cluster sets of the transmit antenna evolve based on the birth-death process, which causes clusters in cluster sets to be divided into two categories: survived clusters and newly generated clusters. The geometrical relationships of surviving clusters are updated according to Eqs. (19)–(23). For newly generated clusters, the distributions of the newly generated clusters are initialized according to the method as mentioned in Section 3.2. After C_l^{T} $(l=1,2,\ldots,M_{\mathrm{T}})$ at time $t+\Delta t$ have been

obtained, the visibility region method proposed in Section 3.2 is used to describe the cluster evolution on the receive antenna array.

4 A corresponding simulation model for the theoretical model

To analyze the spatial-temporal properties of our proposed channel model with cluster evolution on both the array and time axes, the spatial-temporal correlation function will be introduced in this section. Meanwhile, a simulation model with a finite number of rays, which captures channel spatial-temporal properties as accurately as possible, is developed. The spatial-temporal correlation function between the channel gains $h_{kl,n}(t)$ and $h_{k'l',n}(t)$ is defined as

$$\rho_{kl,k'l',n}(\delta_{\mathrm{T}},\delta_{\mathrm{R}},\Delta t;t)=E\left[\frac{h^{*}_{kl,n}(t)h_{k'l',n}(t+\Delta t)}{|h^{*}_{kl,n}(t)||h_{k'l',n}(t+\Delta t)|}\right]. \tag{24}$$

Because the LOS component and NLOS components are independent, Eq. (24) can be rewritten as the sum of the spatial-temporal correlation functions of the LOS component and NLOS component, i.e.,

$$\begin{aligned}&\rho_{kl,k'l',n}(\delta_{\mathrm{T}},\delta_{\mathrm{R}},\Delta t;t)\\&=\rho^{\mathrm{LOS}}_{kl,k'l',n}(\delta_{\mathrm{T}},\delta_{\mathrm{R}},\Delta t;t)+\rho^{\mathrm{NLOS}}_{kl,k'l',n}(\delta_{\mathrm{T}},\delta_{\mathrm{R}},\Delta t;t),\end{aligned} \tag{25}$$

where

$$\rho^{\mathrm{LOS}}_{kl,k'l',n}(\delta_{\mathrm{T}},\delta_{\mathrm{R}},\Delta t;t)=\frac{K\delta(n-1)}{K+1}\exp\left(\mathrm{j}\phi^{\mathrm{LOS}}\right), \tag{26}$$

$$\begin{aligned}&\rho^{\mathrm{NLOS}}_{kl,k'l',n}(\delta_{\mathrm{T}},\delta_{\mathrm{R}},\Delta t;t)\\&=\frac{1}{K\delta(n-1)+1}E\left[\lim_{M\to\infty}\frac{1}{\sqrt{M}}\sum_{i=1}^{M}\exp\left(\mathrm{j}\phi^{\mathrm{NLOS}}\right)\right],\end{aligned} \tag{27}$$

with

$$\begin{aligned}\phi^{\mathrm{LOS}}=&\,2\pi f^{\mathrm{LOS}}_{k'l'}(t+\Delta t)(t+\Delta t)-2\pi f^{\mathrm{LOS}}_{kl}(t)t\\&+\varphi^{\mathrm{LOS}}_{k'l'}(t+\Delta t)-\varphi^{\mathrm{LOS}}_{kl}(t),\end{aligned} \tag{28}$$

$$\begin{aligned}\phi^{\mathrm{NLOS}}=&\,2\pi f^{\mathrm{NLOS}}_{k'l',n,i}(t+\Delta t)(t+\Delta t)-2\pi f^{\mathrm{NLOS}}_{kl,n,i}(t)t\\&+\varphi^{\mathrm{NLOS}}_{k'l',n,i}(t+\Delta t)-\varphi^{\mathrm{NLOS}}_{kl,n,i}(t).\end{aligned} \tag{29}$$

As shown in Eq. (1), the number of rays is infinite in the proposed theoretical channel model. Therefore, the discrete AoDs $\alpha^{\mathrm{T}}_{n,i}$ can be represented by a continuous random variable α^{T}_{n}. Under the given probability density function (PDF) of the AoD $p_{\alpha^{\mathrm{T}}_n}(\alpha^{\mathrm{T}}_n)$, such as a Laplacian distribution, Gaussian distribution, uniform distribution, and von Mises distribution, $\rho^{\mathrm{NLOS}}_{kl,k'l',n}(\delta_{\mathrm{T}},\delta_{\mathrm{R}},\Delta t;t)$ is computed as

$$\rho^{\mathrm{NLOS}}_{kl,k'l',n}(\delta_{\mathrm{T}},\delta_{\mathrm{R}},\Delta t;t)=\int_{-\pi}^{-\pi}\exp(\mathrm{j}\phi^{\mathrm{NLOS}})p_{\alpha^{\mathrm{T}}_n}(\alpha^{\mathrm{T}}_n)\mathrm{d}\alpha^{\mathrm{T}}_n. \tag{30}$$

However, a channel simulator with infinite rays is not practical because of the high complexity of implementation. Therefore, a simulation model that aims at approximating $\rho^{\mathrm{NLOS}}_{kl,k'l',n}(\delta_{\mathrm{T}},\delta_{\mathrm{R}},\Delta t;t)$ with finite and discrete AODs $\alpha^{\mathrm{T}}_{n,i}$ should be discussed. Our proposed method is as follows. Given the PDF that α^{T}_n satisfies in the theoretical channel, the uniform power subpath method is used to calculate the offset angles with the PAS satisfying the same PDF; e.g., if α^{T}_n satisfies the Laplacian distribution, offset angles are calculated under the Laplacian PAS. Then, the $\alpha^{\mathrm{T}}_{n,i}$ will be obtained. As can be imagined, the simulation model will be approximately equal to the theoretical model with enormous rays. Thus, the approximated value can be expressed as

$$\rho^{\mathrm{NLOS}}_{kl,k'l',n}(\delta_{\mathrm{T}},\delta_{\mathrm{R}},\Delta t;t)\approx\frac{1}{M}\sum_{i=1}^{M}\exp(\mathrm{j}\phi^{\mathrm{NLOS}}). \tag{31}$$

5 Numerical results and analysis

In this section, numerical results are provided to analyze and verify the proposed channel model. To perform numerical analysis, corresponding parameters are generated according to Section 3. Assume that the parameters for the birth-death process are the same as those in Wu HL *et al.* (2015). The Laplacian PAS and free space path-loss function are used when calculating the visibility region gain. For the theoretical channel model, the offset angles of rays within the cluster are assumed to obey the Laplacian distribution. Therefore, the PDF of angles of rays within the nth cluster can be expressed as

$$p_{\alpha^{\mathrm{T}}_n}(\alpha^{\mathrm{T}}_n)=\frac{1}{2b}\exp\left(-\frac{|\alpha^{\mathrm{T}}_n-\mu|}{b}\right),\ \alpha^{\mathrm{T}}_n\in(-\pi,\pi], \tag{32}$$

where b is the scale parameter, and μ is the position parameter.

By setting the number of rays $M=20$, an example of the maximum power deviation of rays within the cluster for different antenna pairs is depicted

in Fig. 4. It can be observed that the maximum power deviation is more than 6 dB for the antenna pair $(k,l)=(15,15)$, which may result in some rays within the cluster being invisible to the receive antenna. This shows the necessity for describing non-stationary properties of clusters in terms of rays. Furthermore, by setting the threshold value -100 dB, an example of ray evolution on the array axis is depicted in Fig. 5. There are originally 20 rays (Ray_1 to Ray_{20}) existing within one cluster, and these rays evolve according to their visibility gain. It can be observed that four rays (Ray_{13}, Ray_{15}, Ray_{17}, Ray_{19}) of the original 20 rays are invisible to the first antenna. Ray_{10} is visible to the entire receive antenna array, and Ray_5 is visible to a portion of the receive antenna array. As a result, different antenna elements may observe different rays within one cluster. Additionally, unlike the description of the visibility region from the cluster perspective, the existing rays within the cluster and their parameters are sufficient for computing channel coefficients.

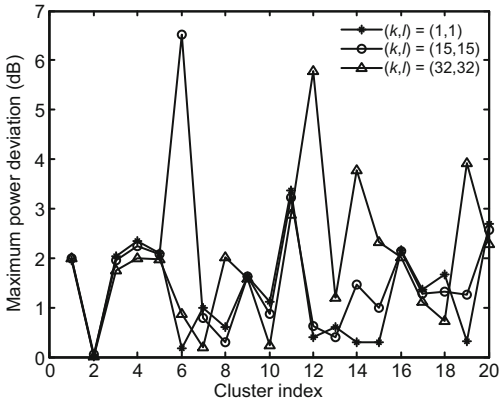

Fig. 4 An example of maximum power deviation of rays within the cluster

By setting $\Delta t=0$, the spatial-temporal correlation function reduces to the spatial cross-correlation function (CCF) $\rho_{kl,k'l',n}(\delta_{\mathrm{T}},\delta_{\mathrm{R}};t)$. Furthermore, if we set $\delta_{\mathrm{T}}=0$, the impact of the number of rays within the cluster on the absolute spatial CCF $|\rho_{11,12,1}(0,\delta_{\mathrm{R}};t)|$ of the receiver is depicted in Fig. 6. The figure shows that the increase in the number of rays results in higher receiver antenna correlations. In addition, the spatial CCF values of the simulation model are approaching those of the theoretical model with an increasing number of rays. Therefore, it shows that the simulation model is able to capture the channel spatial correlation

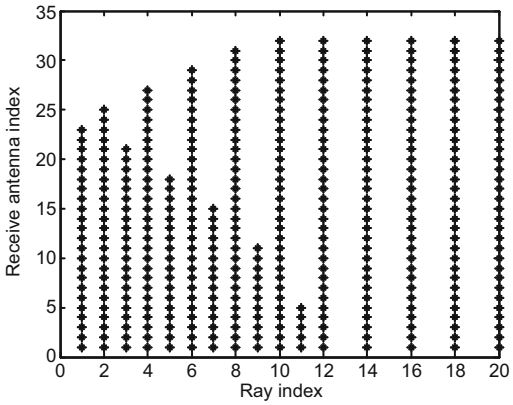

Fig. 5 An example of ray evolution on the receive antenna array (the asterisk symbol in the two-dimensional plane means its corresponding antenna element observes its corresponding ray element)

characteristic with the finite number of rays.

By setting the number of rays $M=80$, the receiver absolute spatial CCF in terms of different values of adjacent antenna (k',k) pairs with $|k'-k|=1$ is depicted in Fig. 7. On one hand, it shows the trend that spatial CCF values slowly decrease as the normalized antenna spacing increases, which is similar to the observation in Wu HL *et al.* (2015). On the other hand, as to $|k'-k|=1$, spatial CCF values are different with different values of k' and k, which shows that the spatial CCF value depends not only on the absolute difference between antenna indices but also on the reference antenna indices. Therefore, WSS properties on the antenna array axis are not valid under the spherical wave-front assumption.

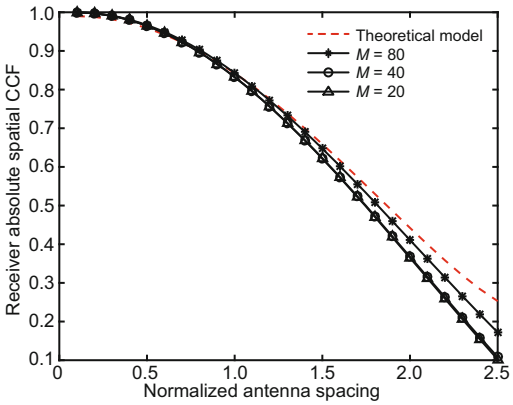

Fig. 6 Absolute receiver spatial cross-correlation function (CCF) $|\rho_{11,12,1}(0,\delta_{\mathrm{R}};t)|$ of the proposed channel model in terms of the number of rays at the receiver side ($M_{\mathrm{R}}=32$, $M_{\mathrm{T}}=1$, $t=1$ s, $D=150$ m, $b=1$, $\mu=0$, $\beta_{\mathrm{T}}=\beta_{\mathrm{R}}=\pi/2$, $\lambda=0.15$ m, $f_{\max}=66.66$ Hz, $\theta_v=\pi/3$, NLOS)

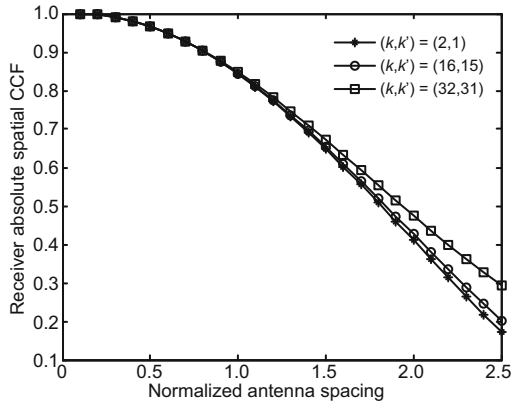

Fig. 7 Absolute receiver spatial cross-correlation function (CCF) $|\rho_{k1,k'1,1}(0,\delta_{\mathrm{R}};t)|$ of the proposed channel model in terms of different values of (k',k) pairs with $|k'-k|=1$ ($M_{\mathrm{R}}=32$, $M_{\mathrm{T}}=1$, $t=1$ s, $D=150$ m, $b=1$, $\mu=0$, $M=80$, $\beta_{\mathrm{T}}=\beta_{\mathrm{R}}=\pi/2$, $\lambda=0.15$ m, $f_{\max}=66.66$ Hz, $\theta_v=\pi/3$, NLOS)

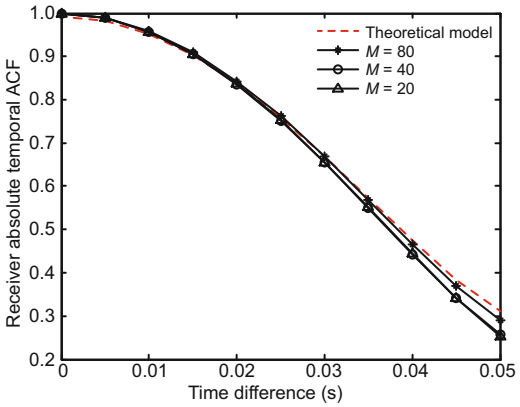

Fig. 8 Absolute receiver temporal auto-correlation function (ACF) $|\rho_{11,1}(\Delta t;t)|$ of the proposed channel model in terms of the number of rays within the cluster at the receiver side ($M_{\mathrm{R}}=32$, $M_{\mathrm{T}}=32$) $t=1$ s, $D=150$ m, $b=1$, $\mu=0$, $\beta_{\mathrm{T}}=\beta_{\mathrm{R}}=\pi/2$, $\lambda=0.15$ m, $f_{\max}=66.66$ Hz, $V_{\mathrm{c}}=1$ m/s, $\theta_{c,n}=\pi/3$, $\theta_v=\pi/3$, NLOS)

Setting $l=l'$ and $k=k'$, the absolute temporal auto-correlation function (ACF) $|\rho_{kl,n}(\Delta t;t)|$, in terms of the number of rays within the cluster at the receiver side, is analyzed in Fig. 8. The figure shows that the temporal ACF decreases more slowly as the number of rays becomes larger, and the increase in the number of rays results in temporal ACF values of the simulation model being more similar to those of the theoretical model. Setting the number of rays $M=80$, the auto-correlation characteristic of a single receive antenna at different times is shown in Fig. 9. Together with updated geometrical relationships and cluster evolution on both the array and time axes, Fig. 9 shows that the temporal ACF value decreases as the time difference increases, demonstrating the temporal non-stationary characteristics of the model.

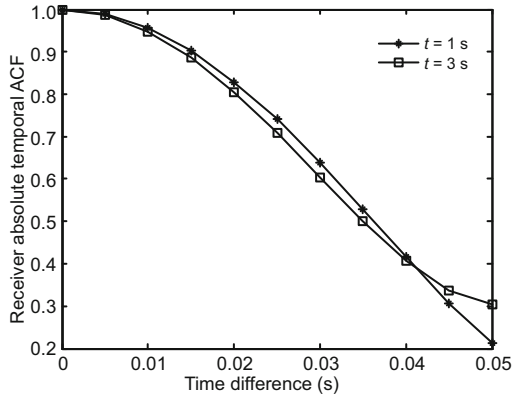

Fig. 9 Absolute temporal auto-correlation function (ACF) of Cluster$_1$ $|\rho_{11,1}(\Delta t;t)|$ of the proposed channel model in terms of time $t=1$ s and $t=3$ s ($M_{\mathrm{R}}=32$, $M_{\mathrm{T}}=32$, $D=150$ m, $b=1$, $\mu=0$, $M=80$, $\beta_{\mathrm{T}}=\beta_{\mathrm{R}}=\pi/2$, $\lambda=0.15$ m, $f_{\max}=66.66$ Hz, $V_{\mathrm{c}}=1$ m/s, $\theta_{c,n}=\pi/3$, $\theta_v=\pi/3$, NLOS)

6 Conclusions

A novel theoretical non-stationary channel model reflecting the spherical wave-front assumption and cluster evolution on both the array and time axes is proposed for massive MIMO. A spherical wave-front has been assumed to capture the characteristics of AoA shifts and Doppler frequency variations because of near-field effects, and expressions for calculating channel coefficients are derived. To describe the non-stationary properties of clusters on both the array and time axes, we propose a novel visibility region method that models cluster evolution in terms of the ray visibility gain. Combining this visibility region with the birth-death process, a novel cluster evolution algorithm is presented. Additionally, the impacts of cluster evolution and the spherical wave-front assumption on the statistical properties of the channel model are investigated. A simulation model corresponding to the theoretical model is also proposed, and simulation results show that the channel characteristics of the simulation model are consistent with those of the theoretical model. Consequently, our proposed channel model, which captures the important channel features of massive MIMO channels, can serve as a design framework to model massive MIMO channels.

References

Babich, F., Lombardi, G., 2000. A Markov model for the mobile propagation channel. *IEEE Trans. Veh. Technol.*, **49**(1):63-73. https://doi.org/10.1109/25.820699

Bohagen, F., Orten, P., Oien, G.E., 2006. Modeling of line-of-sight 2×2 MIMO channels: spherical versus plane waves. IEEE Int. Symp. on Personal, Indoor and Mobile Radio Communications, p.1-5. https://doi.org/10.1109/PIMRC.2006.254307

Chong, C.C., Tan, C.M., Laurenson, D.I., *et al.*, 2005. A novel wideband dynamic directional indoor channel model based on a Markov process. *IEEE Trans. Wirel. Commun.*, **4**(4):1539-1552. https://doi.org/10.1109/TWC.2005.850341

ETSI, 2014. Spatial Channel Model for Multiple Input Multiple Output (MIMO). Technical Report, 3GPP TR 25.996 Release 12. http://www.3gpp.org

Gao, X., Tufvesson, F., Edfors, O., *et al.*, 2012. Measured propagation characteristics for very-large MIMO at 2.6 GHz. 46th Asilomar Conf. on Signals, Systems and Computers, p.295-299. https://doi.org/10.1109/ACSSC.2012.6489010

Gao, X., Tufvesson, F., Edfors, O., 2013. Massive MIMO channels—measurements and models. Asilomar Conf. on Signals, Systems and Computers, p.280-284. https://doi.org/10.1109/ACSSC.2013.6810277

ITU-R, 2008. Guidelines for Evaluation of Radio Interface Technologies for IMT-Advanced. Technical Report, No. M.2135.

Kyösti, P., Meinilä, J., Hentilä, L., *et al.*, 2007. Winner II Channel Models Part II Radio Channel Measurement and Analysis Results. Technical Report, No. T-4-027756.

Larsson, E.G., Edfors, O., Tufvesson, F., *et al.*, 2014. Massive MIMO for next generation wireless systems. *IEEE Commun. Mag.*, **52**(2):186-195. https://doi.org/10.1109/MCOM.2014.6736761

Li, X.R., Zhou, S.D., Bjornson, E., *et al.*, 2015. Capacity analysis for spatially non-wide sense stationary uplink massive MIMO systems. *IEEE Trans. Wirel. Commun.*, **14**(12):7044-7056. https://doi.org/10.1109/TWC.2015.2464219

Liu, L.F., Oestges, C., Poutanen, J., *et al.*, 2012. The cost 2 100 MIMO channel model. *IEEE Wirel. Commun.*, **19**(6):92-99. https://doi.org/10.1109/MWC.2012.6393523

Lu, L., Li, G.Y., Swindlehurst, A.L., *et al.*, 2014. An overview of massive MIMO: benefits and challenges. *IEEE J. Sel. Top. Signal Process.*, **8**(5):742-758. https://doi.org/10.1109/JSTSP.2014.2317671

Paetzold, M., 2011. Mobile Radio Channels (2nd Ed). John Wiley and Sons, West Sussex, UK.

Payami, S., Tufvesson, F., 2012. Channel measurements and analysis for very large array systems at 2.6 GHz. 6th European Conf. on Antennas and Propagation, p.433-437. https://doi.org/10.1109/EuCAP.2012.6206345

Rusek, F., Persson, D., Lau, B.K., *et al.*, 2013. Scaling up MIMO: opportunities and challenges with very large arrays. *IEEE Signal Process Mag.*, **30**(1):40-60. https://doi.org/10.1109/MSP.2011.2178495

Schumacher, L., Pedersen, K.I., Mogensen, P.E., 2002. From antenna spacings to theoretical capacities—guidelines for simulating MIMO systems. 13th IEEE Int. Symp. on Personal, Indoor and Mobile Radio Communications, p.587-592. https://doi.org/10.1109/PIMRC.2002.1047289

Wang, C.X., Haider, F., Gao, X.Q., *et al.*, 2014. Cellular architecture and key technologies for 5G wireless communication networks. *IEEE Commun. Mag.*, **52**(2):122-130. https://doi.org/10.1109/MCOM.2014.6736752

Wu, H.L., Jin, S., Gao, X.Q., 2015. Non-stationary multi-ring channel model for massive MIMO systems. Int. Conf. on Wireless Communications & Signal Processing, p.1-6. https://doi.org/10.1109/WCSP.2015.7341264

Wu, S.B., Wang, C.X., Aggoune, E.H.M., *et al.*, 2014. A non-stationary 3D wideband twin-cluster model for 5G massive MIMO channels. *IEEE J. Sel. Areas Commun.*, **32**(6):1207-1218. https://doi.org/10.1109/JSAC.2014.2328131

Wu, S.B., Wang, C.X., Haas, H., *et al.*, 2015. A non-stationary wideband channel model for massive MIMO communication systems. *IEEE Trans. Wirel. Commun.*, **14**(3):1434-1446. https://doi.org/10.1109/TWC.2014.2366153

Xie, Y., Li, B., Zuo, X.Y., *et al.*, 2015. A 3D geometry-based stochastic model for 5G massive MIMO channels. Int. Conf. on Heterogeneous Networking for Quality, Reliability, Security and Robustness, p.216-222. https://doi.org/10.4108/eai.19-8-2015.2259755

Yaghjian, A.D., 1986. An overview of near-field antenna measurements. *IEEE Trans. Antennas Propag.*, **34**(1):30-45. https://doi.org/10.1109/TAP.1986.1143727

Zheng, K., Ou, S.L., Yin, X.F., 2014. Massive MIMO channel models: a survey. *Int. J. Antennas Propag.*, **2014**(11):1-10. https://doi.org/10.1155/2014/848071

Zwick, T., Fischer, C., Didascalou, D., *et al.*, 2000. A stochastic spatial channel model based on wave-propagation modeling. *IEEE J. Sel. Areas Commun.*, **18**(1):6-15. https://doi.org/10.1109/49.821698

Zwick, T., Fischer, C., Wiesbeck, W., 2002. A stochastic multipath channel model including path directions for indoor environments. *IEEE J. Sel. Areas Commun.*, **20**(6):1178-1192. https://doi.org/10.1109/JSAC.2002.801218